Persistent currents in carbon nanotori: Effects of structure deformations and chirality

Zhenhua Zhang, Jianhui Yuan, Ming Qiu, Jingcui Peng, and Fuliang Xiao

Citation: Journal of Applied Physics **99**, 104311 (2006); doi: 10.1063/1.2199981
View online: https://doi.org/10.1063/1.2199981
View Table of Contents: http://aip.scitation.org/toc/jap/99/10
Published by the American Institute of Physics

Persistent currents in carbon nanotori: Effects of structure deformations and chirality

Zhenhua Zhang[a)]
Surface Physics Laboratory (National Key Laboratory), Fudan University, Shanghai 200433, China and Department of Physics and Electronic Science, Changsha University of Science and Technology, Changsha 410076, China

Jianhui Yuan and Ming Qiu
Department of Physics and Electronic Science, Changsha University of Science and Technology, Changsha 410076, China

Jingcui Peng
Department of Applied Physics, Hunan University, Changsha 410082, China

Fuliang Xiao
Department of Physics and Electronic Science, Changsha University of Science and Technology, Changsha 410076, China

(Received 9 February 2005; accepted 29 March 2006; published online 30 May 2006)

The persistent currents as a function of the dimension, chirality, and deformation for various chiral carbon nanotori are investigated theoretically. It has been found that, for the undeformed torus, its persistent current is inversely proportional to the torus radius R, but independent of the torus width r, and becomes very strong as its chiral angle θ approaches $\pm 15°$; whereas for the deformed torus, its energy gap E_g and persistent current are very sensitive to the deformation and chirality. In general, the persistent current can be fitted to the form $I=\pm A\sin(2\pi\Phi/\Phi_0)$ as long as the deformation occurs except in the case of $\tan\alpha=0$ and $\varepsilon_L=\varepsilon_J$, where Φ is the magnetic flux enclosed in the torus, $\Phi_0(=h/e)$ is the flux quantum, α represents the shear strain, and ε_L and ε_J denote the strains due to tension or compression along the directions of tube and torus circumferences, respectively. When the strain reaches 1%, the persistent current declines by four orders of magnitude. © *2006 American Institute of Physics*. [DOI: 10.1063/1.2199981]

I. INTRODUCTION

Carbon nanotubes have been extensively studied since their discovery in 1991 because their conductivity may be either metallic or semiconducting depending on their geometrical structure, especially on their chirality. These unique electronic properties are expected to have unprecedented practical applications in future nanoelectronics for developing small electronic devices.[1–7]

The carbon nanotorus, as an important member of the family of carbon clusters, was theoretically proposed by Dunlap,[8] followed by Itoh *et al.*,[9] and observed experimentally in 1992.[10] Its structure is considered theoretically to connect small sliced parts of the nanotube through the pairs of pentagons and heptagons. Instead, another structure of the carbon nanotorus is formed by means of bending a carbon nanotube and connecting its two ends together without introducing the pairs of pentagons and heptagons. Such a nanotube, of course, should be sufficiently long. Recently, a number of studies have been reported on synthesized techniques,[11–14] experimental measurements,[15,16] and theoretical calculations[17–24] of the carbon ring (or torus). Its various properties, such as the conducting behavior,[16] the negative magnetoresistance and weak electron-electron interaction in the low temperature regime,[15] the unique atomic and electronic structures,[18,22–24] the deformation and defective effects of electronic structure,[23,25] the magnetic response,[17–21] the persistent current,[20,26] etc., have been discussed extensively.

Currently, the theoretical researches on the electronic structures of the carbon nanotori are mainly concentrated on the simple achiral cases (armchair-zigzag and zigzag-armchair tori),[20,23,25] and their persistent currents are calculated only for the undeformed and achiral tori.[20,26] In fact, various deformations are inevitably incorporated in realistic chiral carbon nanotorus during its growth, deposition, processing, and manipulation. Therefore, the investigation of the effects of chirality and deformation on the electronic structure and the persistent current for the chiral carbon nanotorus is very necessary.

In this paper, we deduce the electronic structure of the deformed chiral carbon nanotorus first, then calculate the persistent currents in the coherent regime by focusing mainly on the effects of chirality and structural deformation, which is supposed to be homogeneous and elastic. The results show that the energy gap and persistent current of the deformed torus are very sensitive to the deformation and chirality. Generally, the persistent current can be fitted to the form $I=\pm A\sin(2\pi\Phi/\Phi_0)$ as long as the deformation occurs except in some special case. When the strain reaches 1%, the persistent current declines by four orders of magnitude. This drastic reduction of persistent current caused by the symmetry-breaking effect under the deformation suggests

a)Author to whom correspondence should be addressed; electronic mail: huazhenzhang@tom.net

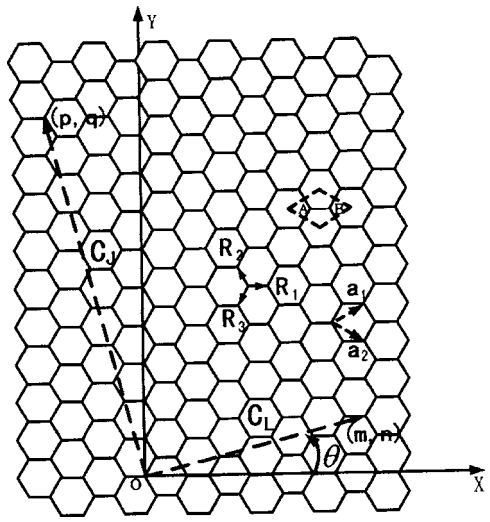

FIG. 1. The unrolled honeycomb lattice of a graphite sheet. The transverse vector $\boldsymbol{C_L}=m\boldsymbol{a}_1+n\boldsymbol{a}_2$ and the longitudinal vector $\boldsymbol{C_J}=p\boldsymbol{a}_1+q\boldsymbol{a}_2$ correspond to the tube and torus circumferences, respectively. $\boldsymbol{a}_1$ and $\boldsymbol{a}_2$ are the unit vectors of a graphite sheet. $\boldsymbol{R}_1$, $\boldsymbol{R}_2$, and $\boldsymbol{R}_3$ denote the vectors of bond lengths. θ is the chiral angle. The unit cell of graphite sheet contains two different carbon atoms, A and B.

that the carbon nanotorus electromechanical system may possess important potential applications for making physical sensors (e.g., pressure sensors).

II. ELECTRONIC STRUCTURE OF CARBON NANOTORUS

The tight-binding model with one π-electron per atom is a useful method for describing the electronic structures of graphene,[27] carbon nanotubes,[28,29] and undeformed achiral carbon nanotorus.[20,26] In this study, we will use this method to investigate the electronic structure of deformed chiral carbon nanotorus. The tight-binding Hamiltonian used is in the form of[30–33]

$$H=-\sum_{l,\rho}\gamma_{l,l+\rho}\exp\left(i\frac{e}{\hbar}\int_{\boldsymbol{R}_l}^{\boldsymbol{R}_{l+\rho}}\boldsymbol{A}\cdot d\boldsymbol{l}\right)C_l^{+}C_{l+\rho}, \tag{1}$$

where $C_l^{+}(C_{l+\rho})$ is the creation operator (annihilator) of electron, the index ρ is counted only for the nearest-neighbor atoms, and $\boldsymbol{A}$ is the vector potential of a uniform magnetic field $\boldsymbol{B}$. All transfer integrals $\gamma_{l,l+\rho}$ depend only on the bond length of the graphite sheet.[34] If the atomic position R_l (for atom A in Fig. 1) is given, then we take $R_{l+\rho}-R_l=R_\rho$ and $\gamma_{l,l+\rho}=\gamma_\rho$ for short, where ρ corresponds to the three nearest-neighbor atoms B shown in Fig. 1.

A single carbon nanotorus may be described as a long rolled-up graphite sheet bent around to the form of torus (see Fig. 1). The transverse vector $\boldsymbol{C_L}=m\boldsymbol{a}_1+n\boldsymbol{a}_2$ and the longitudinal vector $\boldsymbol{C_J}=p\boldsymbol{a}_1+q\boldsymbol{a}_2$ correspond to the tube and torus circumferences, respectively. A carbon nanotorus can be uniquely defined by four integer indices m, n, p, and q as (m,n,p,q), for which the relations $(2m+n)p+(m+2n)q=0$ and $|\boldsymbol{C_J}|\gg|\boldsymbol{C_L}|$ are satisfied. In the case of a deformed graphite sheet, we use ε_L and ε_J to denote the strains caused by the tension or compression along the directions of $\hat{\boldsymbol{C}}_{\boldsymbol{L}}$ and $\hat{\boldsymbol{C}}_{\boldsymbol{J}}$, respectively, where $\hat{\boldsymbol{C}}_{\boldsymbol{L}}$ and $\hat{\boldsymbol{C}}_{\boldsymbol{J}}$ are the unit vectors of $\boldsymbol{C_L}$ and $\boldsymbol{C_J}$. The torsion deformation $\tan\alpha$ is assumed to appear only around the straight tubular axis ($\|\boldsymbol{C_J}$) before bending carbon nanotubes to form torus, where α represents the shear strain. When various deformations occur simultaneously, the two components of arbitrary lattice vector, $\boldsymbol{R}_l=R_{lL}\hat{\boldsymbol{C}}_{\boldsymbol{L}}+R_{lJ}\hat{\boldsymbol{C}}_{\boldsymbol{J}}$, transform to $R_{lJ}\rightarrow(1+\varepsilon_J)R_{lJ}$ and $R_{lL}\rightarrow(1+\varepsilon_L)R_{lL}+R_{lJ}\tan\alpha$. The unit vectors $\boldsymbol{a}_1$ and $\boldsymbol{a}_2$ can be expressed in turn as a function of deformation parameters $(\varepsilon_L,\varepsilon_J,\tan\alpha)$ and chirality.

When a finite graphite sheet, whether deformed or not, is rolled up to form a carbon nanotorus, the periodical boundary conditions along both the transverse and longitudinal directions must be considered. At low temperature, if the electronic phase coherence in this structure is preserved on a length scale comparable to or larger than the torus circumference, then the electronic structure of this nanotorus remains fully described by the eigenfunction of its Hamiltonian. Assume that a homogeneous magnetic field $\boldsymbol{B}$ is applied through the torus plane, that is, its potential vector $\boldsymbol{A}$ is parallel to the longitudinal direction. Using the periodical boundary conditions $\Psi(\boldsymbol{r})=\Psi(\boldsymbol{r}+\boldsymbol{C}_i)$ $(i=L,J)$, where $\Psi(\boldsymbol{r})$ is the electron's Bloch function, and L and J are integers representing the electronic state index, the two components k_x and k_y of the quantized wave vector $\boldsymbol{k}$ can be expressed as a function of deformation, chirality, and magnetic flux.

Based on Eq. (1) and the above description, we obtain the following unified expression of π-electron energy states for the carbon nanotorus as a function of chirality, deformations, and magnetic flux through the torus plane:

$$\begin{aligned}E^{(L,J)}(\Phi,\varepsilon_L,\varepsilon_J,\tan\alpha)=\pm\Bigg(&\sum_{o=l}^{3}\gamma_\rho^2+2\gamma_1\gamma_2\cos\left\{\frac{2\pi}{pn-qm}[pL-m(J+\Phi/\Phi_0)]\right\}\\&+2\gamma_1\gamma_3\cos\left\{\frac{2\pi}{pn-qm}[-qL+n(J+\Phi/\Phi_0)]\right\}\\&+2\gamma_2\gamma_3\cos\left\{\frac{2\pi}{pn-qm}[-(p+q)L+(m+n)(J+\Phi/\Phi_0)]\right\}\Bigg)^{1/2},\end{aligned} \tag{2}$$

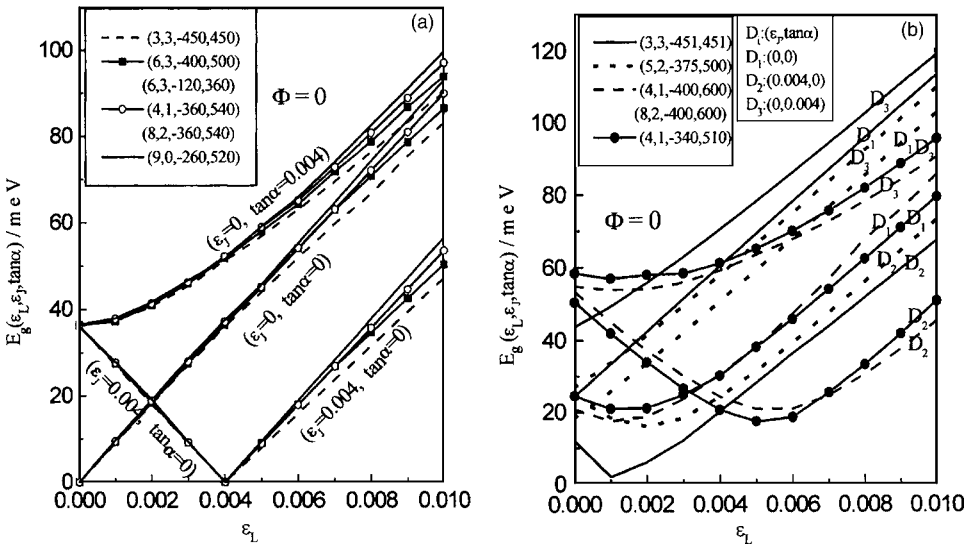

FIG. 2. The deformation-dependent energy gaps $E_g(\varepsilon_L,\varepsilon_J,\tan\alpha)$ for various carbon nanotori. (a) Metallic (type I) tori, where E_g display identical changing features vs the deformation parameters $(\varepsilon_L,\varepsilon_J,\tan\alpha)$ and depend strongly on the deformation and weakly on the chirality. When $\tan\alpha=0$ and $\varepsilon_L=\varepsilon_J$, the metallic nanotorus retains its metallic characteristic. (b) Semiconducting (type II) tori, where E_g depend strongly on deformation and chirality, without distinctive regularity.

where Φ is the magnetic flux and $\Phi_0(=h/e)$ is the flux quantum. Φ includes the magnetic fluxes penetrating both the area of the hole and the bulk of the torus, namely, $\Phi=\Phi_{\text{bulk}}+\Phi_{\text{hole}}\approx 4\pi rRB+\pi(R-r)^2B$, and $\Phi_{\text{bulk}}/\Phi_{\text{hole}}=4rR/(R-r)^2\approx 4r/R=4|\boldsymbol{C_L}|/|\boldsymbol{C_J}|$, where R and r are the torus radius and tube radius (torus width), respectively. Since $|\boldsymbol{C_J}|\gg|\boldsymbol{C_L}|$ as stated above, if we choose $R\sim 200$ Å and $r\sim 2$ Å for a torus studied in this paper, the magnetic flux penetrating the bulk of the torus can be neglected rationally. It is very interesting to note that the electronic energy states of such complicatedly deformed nanotorus system can be described through a surprisingly concise expression and are affected by deformation only through the transfer integral γ_ρ, rather than the electronic phase factor $\boldsymbol{k}\cdot\boldsymbol{R}_\rho$ contained in Eq. (1), although both $\boldsymbol{k}$ and $\boldsymbol{a_i}$ are complicated functions of the deformed parameters $(\varepsilon_L,\varepsilon_J,\tan\alpha)$. Furthermore, we can obtain $E^{(L,J)}(\Phi/\Phi_0,\varepsilon_L,\varepsilon_J,\tan\alpha)=E^{(L,J-l)}(\Phi/\Phi_0+l,\varepsilon_L,\varepsilon_J,\tan\alpha)$, which indicates that $E^{(L,J)}(\Phi/\Phi_0,\varepsilon_L,\varepsilon_J,\tan\alpha)$ is a periodical function of the magnetic flux Φ with a period Φ_0. In addition, the interaction energy between spin and magnetic field (the Zeeman splitting) in Eq. (2) is neglected because it is very small compared with the subband level spacing in the case of weak magnetic flux $(\Phi\sim\Phi_0)$.[35] For a deformed structure, the transfer integral γ_ρ is simply related to the bond length by $\gamma_\rho=\gamma_0(R_0/R_\rho)^2$,[34] where $\gamma_0(=2.66$ eV) and $R_0(=0.142$ nm) are the transfer integral and bond length of undeformed structure, respectively, and R_ρ is the bond length in the deformed structure and satisfies $R_\rho=\sqrt{R_{\rho L}^2+R_{\rho J}^2}$ for the graphite sheet. The expressions of $R_{\rho L}$ and $R_{\rho J}$ can be derived from the deformed configuration as follows:

$$R_{1L}=\lambda[\sqrt{3}(m+n)(1+\varepsilon_L)+(n-m)\tan\alpha],\quad R_{1J}=\lambda(n-m)(1+\varepsilon_J), \tag{3a}$$

$$R_{2L}=\lambda[-\sqrt{3}n(1+\varepsilon_L)+(2m+n)\tan\alpha],\quad R_{2J}=\lambda(2m+n)(1+\varepsilon_J), \tag{3b}$$

$$R_{3L}=\lambda[-\sqrt{3}m(1+\varepsilon_L)+(m+2n)\tan\alpha],\quad R_{3J}=\lambda(m+2n)(1+\varepsilon_J), \tag{3c}$$

where $\lambda=a/6\sqrt{3(m^2+n^2+nm)}$ with the lattice constant $a=2.48$ Å of a graphite sheet. From Eq. (2), it is very easy to obtain the results in Refs. 20 and 21 for those simple cases.

The torus may be classified into the metallic (type I), semiconducting (type II), and insulating (type III), depending entirely on the gap between the highest occupied molecular orbital and the lowest unoccupied molecular orbital in the proximity of Fermi level. In the absence of deformation and magnetic field, using Eq. (2) we deduce a simple rule, viz., the chiral metallic carbon nanotorus satisfies $m-n=3i$ and $p-q=3j$ (i and j are integers), the chiral semiconducting torus satisfies $m-n=3i$ and $p-q\neq 3j$, and the chiral insulating torus satisfies $m-n\neq 3i$ and $p-q=3j$. It can also be verified that the torus with $m-n\neq 3i$ and $p-q\neq 3i$ does not exist.

In the absence of magnetic flux, the calculations using Eq. (2) have been performed to explore the correlations between the deformation-dependent energy gap E_g and related parameters, such as deformed parameters $(\varepsilon_L,\varepsilon_J,\tan\alpha)$, torus radius R, tube radius r, and chiral angle θ.

For the metallic carbon nanotori, we choose six tori as model systems with following indices and sizes: (3,3,−450,450) ($r=2.0$ Å, $R=177.4$ Å, $\theta=0°$), (6,3,−400,500) ($r=3.12$ Å, $R=180.6$ Å, $\theta=10.9°$), (4,1,−360,540) ($r=1.8$ Å, $R=187$ Å, $\theta=19.1°$), (9,0,−260,520) ($r=3.55$ Å, $R=177.5$ Å, $\theta=30°$), (8,2,−360,540) ($r=3.6$ Å, $R=187.7$ Å, $\theta=19.1°$), and (6,3,−120,360) ($r=3.12$ Å, $R=125.2$ Å, $\theta=10.9°$). The properties of deformation-dependent energy gaps E_g are shown in Fig. 2(a). Several points should be indicated. (1) The energy gaps of various metallic nanotori display almost identical features related to the deformation parameters $(\varepsilon_L,\varepsilon_J,\tan\alpha)$ and depend strongly on the values of ε_L, ε_J, and $\tan\alpha$. Only when $\tan\alpha=0$ and $\varepsilon_L=\varepsilon_J$, the metallic nanotorus retains its metallic characteristic ($E_g=0$) in spite of the existence of tension deformation. This is because the tension deformation in this case although does change the bond

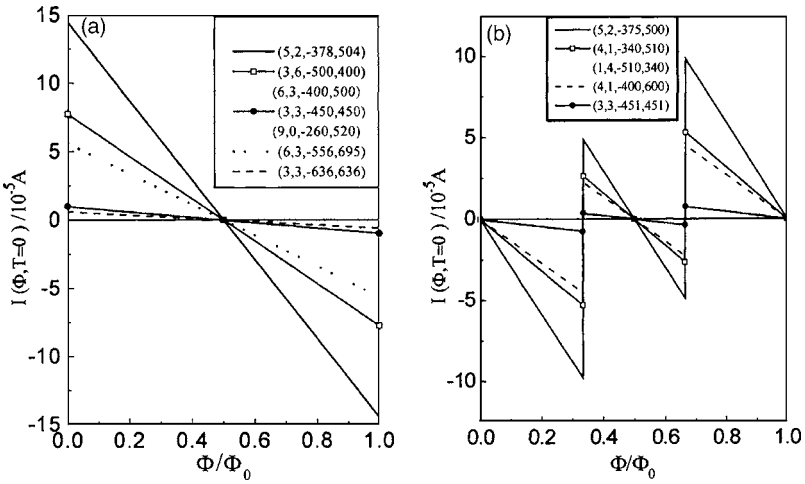

FIG. 3. The persistent currents in (a) the metallic tori and (b) the semiconducting tori at $T=0$ K. They have very significant chiral effects and are inversely proportional to the torus radius R but independent of the torus width r. The maximum values appear in carbon nanotori with θ approaching $\pm 15°$.

lengths but not change the hexagonal symmetry of the honeycomb lattice. As long as setting $\tan\alpha \neq 0, E_g$ is always nonzero, since the torsion deformation always breaks the symmetry of the graphite lattice. (2) E_g depends weakly on the chiral angle θ. It increases slightly with the increasing of θ, indicating that the deformations have less effects on the metallic armchair-zigzag torus ($\theta=0$). In addition, we find that E_g is independent of the torus radius R and width r.

For the semiconducting carbon nanotori, we take five model systems: $(5,2,-375,500)$ ($r=2.5$ Å, $R=177.7$ Å, $\theta=13.9°$), $(4,1,-340,510)$ ($r=1.8$ Å, $R=177.7$ Å, $\theta=19.1°$), $(3,3,-451,451)$ ($r=2.0$ Å, $R=177.8$ Å, $\theta=0°$), $(4,1,-400,600)$ ($r=1.8$ Å, $R=208.6$ Å, $\theta=19.1°$), and $(8,2,-400,600)$ ($r=3.6$ Å, $R=208.6$ Å, $\theta=19.1°$) as examples. The properties of the deformation-dependent energy gaps E_g, shown in Fig. 2(b), can be concluded as follows. (1) E_g shows a strong dependence on the magnitude of ε_L, ε_J, and $\tan\alpha$ and increases or decreases stochastically with the deformation. Setting $\tan\alpha=0$ and $\varepsilon_L=\varepsilon_J$, E_g becomes smaller than that in the undeformed case, but the smallest E_g might occur at some particular values of ε_L and ε_J. If the torsion deformation is involved, E_g is always larger than that in the undeformed case. (2) E_g is independent of torus width r but depends on the chiral angle θ and torus radius R.

III. PERSISTENT CURRENT IN A CHIRAL CARBON NANOTORUS

When a magnetic field is applied, it would yield the change of $\boldsymbol{k}$ value in the Brillouin zone, leading to the variation of electronic states and free energy. For noninteracting electronic system, the persistent current can be obtained by[36]

$$I(\Phi,\varepsilon_L,\varepsilon_J,\tan\alpha,T) = -\left[\frac{\partial F(\Phi,\varepsilon_L,\varepsilon_J,\tan\alpha,T)}{\partial\Phi}\right]_N, \qquad (4)$$

where N is the number of particles in the system, T is the temperature, and $F(\Phi,\varepsilon_L,\varepsilon_J,\tan\alpha,T)$ is the free energy of torus system. The expression for the free energy is

$$F(\Phi,\varepsilon_L,\varepsilon_J,\tan\alpha,T) = -\sum_{LJ\sigma} k_B T \ln\left\{1+\exp\left[\frac{E_F - E^{(L,J)}_{(\Phi,\varepsilon_L,\varepsilon_J,\tan\alpha)}}{k_B T}\right]\right\}, \qquad (5)$$

where k_B is the Boltzmann constant, E_F is the Fermi level, and σ denotes the two states with up and down electron spins. Without doping in the torus, E_F is taken approximately to be zero for any T and magnetic field.

A. Persistent currents in undeformed chiral carbon nanotorus

Using Eqs. (2)–(5)and taking $\varepsilon_L=\varepsilon_J=\tan\alpha=0$, the properties of the calculated persistent currents in various undeformed chiral carbon nanotori and their dependence on the chirality, radius, and width of torus at zero or nonzero temperature can be obtained.

1. Type I metallic torus

The electrons occupy the states of $E^{(L,J)}_{(\Phi)} \leqslant E_F=0$ at $T=0$ K. The calculated persistent currents in this torus type are shown in Fig. 3(a). The results show the following behaviors.

(1) The persistent currents are linearly periodic function of flux Φ with period Φ_0 and antisymmetric about $\Phi_0/2$ for all chiral tori, zigzag-armchair (ZA) torus, and armchair-zigzag (AZ) torus. At $\Phi_c=i\Phi_0$ (i is an integer), the persistent current changes abruptly and shows the special jumps. These discontinuous jumps are intimately related to the metal-semiconductor transition or vice versa. For metallic phase, $E^{(L,J)}_{(\Phi_c)}=0$, thus the persistent currents having singularity at the magnetic flux Φ_c can be derived from Eq. (4).

(2) The chirality affects the persistent current obviously. In Fig. 3(a), the five tori we choose, M1 $(5,2,-378,504)$, M2 $(3,6,-500,400)$, M3 $(6,3,-400,500)$, M4 $(3,3,-450,450)$, and M5 $(9,0,-260,520)$, have almost identical radii ($R\sim 180$ Å). The curves of the persistent currents in AZ torus M4 ($\theta=0°$) and ZA torus M5 ($\theta=30°$) overlap entirely and their values are very small, but the persistent currents in chiral torus M1

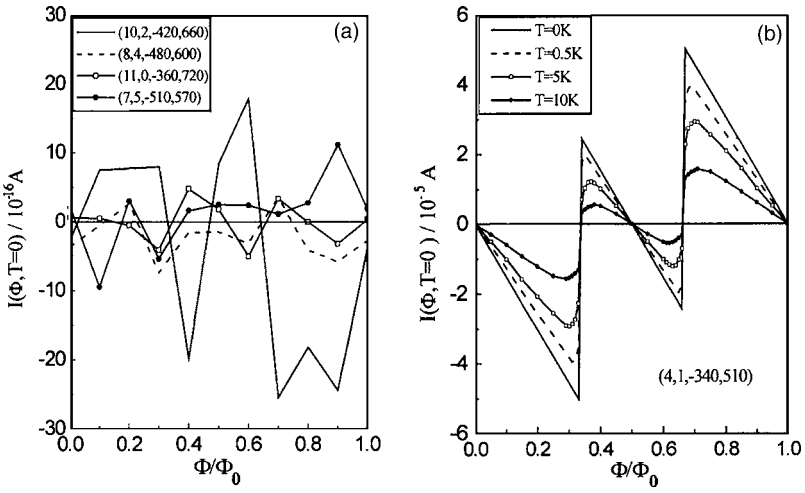

FIG. 4. The persistent currents in (a) type III torus at $T=0$ K. They are of 12–13 orders of magnitude smaller than that in type I and II tori with the same values of R, r, and θ, and in (b) type II torus at finite temperature. They decrease apparently and the sawtooth shape becomes smoother with increasing temperature.

($\theta=13.9°$) are much larger than that in the ZA (or AZ) torus. Moreover, chiral tori M3 ($\theta=-10.9°$) and M2 ($\theta=10.9°$) have the same persistent current. It means that the same persistent current would be yielded in both chiral tori with angles θ and $-\theta$ as long as their radii are the same. It is also found that the persistent current becomes very strong as θ approaches ±15°, because more electronic states contribute to yield persistent currents in torus with this chiral angle.

(3) The magnitude of torus radius has significant effect on the persistent current. As shown in Fig. 3(a), for different tori with the same θ, the larger the torus radius is, the weaker the persistent current is. The relation between the persistent current and torus radius R satisfies $I \propto 1/R$.

(4) The persistent currents are unaffected by the magnitude of torus width r. For example, both $(4,1,-360,540)$ and $(8,2,-360,540)$ chiral tori have the same R and θ, but different r. The calculation shows that their persistent currents always display the same value when the flux Φ changes (not shown here). In this sense, the carbon nanotorus behaves like real one-dimension systems.

2. Type II semiconducting torus

The persistent currents at $T=0$ K are shown in Fig. 3(b), where $(5,2,-375,500)$, $(4,1,-340,510)$, $(1,4,-510,340)$, and $(3,3,-451,451)$ tori have approximately equal radius ($R \sim 180$ Å) but different θ (see the above text). Whereas $(4,1,-400,600)$ torus has the larger radius ($R \sim 210$ Å). The evolution of the persistent currents versus flux Φ in this torus type is linearly periodic with period Φ_0 and antisymmetric about $\Phi_0/2$. The relation between persistent current and R, r, θ for this torus type is the same as type I torus in spite of the different forms of their current curves. However, the persistent currents in type II torus are obviously weaker than that in type I torus. At $\Phi_c=(i\pm 1/3)\Phi_0$, abrupt jumps of the persistent currents in the curves occur, which are also related to the metal-semiconductor transitions or vice versa.

Although the free energy $F(\Phi,T=0)$ in the absence of deformation is a complicated function of Φ, R, r, and θ, the persistent currents $I(\Phi,T=0)$ in type I and II tori can be expressed by a simple equation to reflect the influence of different variables:

$$I(\Phi,T=0) = I(\theta,r,R,\Phi,T=0) = \frac{f(\theta,\Phi,T=0)}{R} = \frac{f(-\theta,\Phi,T=0)}{R}, \tag{6}$$

where $f(\theta,\Phi,T=0)$ is only related to chiral angle θ and magnetic flux Φ. Equation (6) means that the persistent current is inversely proportional to R but independent of r, in agreement with the result in Ref. 26. But the very significant chiral effects on the persistent current and its maximum value appearing in those carbon nanotori with θ approaching ±15° are our main finding in this study. From this viewpoint, the carbon nanotorus is quite different from the featureless metallic or other mesoscopic tori.

3. Type III insulating torus

The persistent currents at $T=0$ K are shown in Fig. 4(a). Typically, the persistent currents in type III torus are of 12–13 orders of magnitude weaker than that in type I and II tori if their R are the same. This is due to the large energy gap of type III torus and the absence of metal-semiconductor transition under the applied magnetic field. The regularity of the persistent currents varying with R, r, and θ cannot be found in this torus type.

4. Effect of temperature

$(4,1,-340,600)$ semiconducting chiral torus is chosen as a model system to study the variation of persistent current versus the temperature. The calculated results are shown in Fig. 4(b). The persistent currents decrease apparently and the sawtooth shapes become smoother as the temperature rises. The reason is that with the temperature increasing more states above the Fermi level are occupied by the electrons, resulting in the partial cancellation of the persistent currents contributed by the conduction band electrons and that contributed by the valence band electrons.

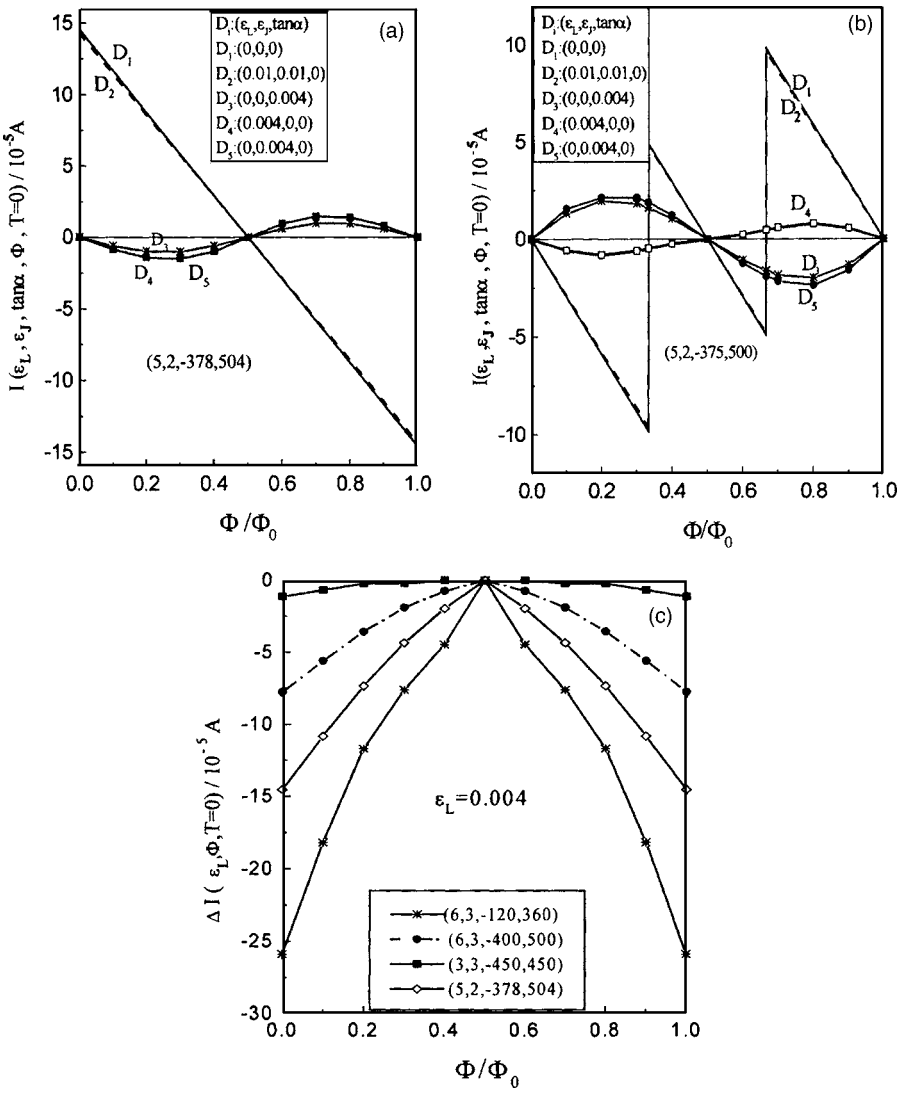

FIG. 5. The persistent currents in deformed carbon nanotori. (a) Metallic torus, and (c) semiconducting torus. The persistent currents in both torus types are very sensitive to deformations. If taking $\tan\alpha=0$ and $\varepsilon_L=\varepsilon_J$, the persistent currents remain almost unchanged as compared with the undeformed torus. While deformation occurs, the jump structure of the persistent currents should become smooth and their curves can be fitted to the form $I=\pm A\sin(2\pi\Phi/\Phi_0)$. Plot (b) shows the dependence of increment of persistent current in various metallic tori on the torus chirality and radius R after deformation occurs.

B. Persistent currents in deformed chiral carbon nanotorus

We now turn to investigate the persistent currents changing with the magnetic flux Φ, deformation parameters $(\varepsilon_L,\varepsilon_J,\tan\alpha)$, and geometrical parameters (R,r,θ) for a deformed carbon nanotorus. For the deformed type I torus, we take $(5,2,-378,504)$ metallic chiral torus as a model system. The obtained persistent currents at zero temperature are shown in Fig. 5(a), where the plot of the persistent currents in the absence of deformations is also drawn for comparison. It is easy to see that the persistent currents are very sensitive to deformations and would yield a substantial drop while the deformation parameters reach 0.4%, that is, $\varepsilon_L=0.004$, or $\varepsilon_J=0.004$, or $\tan\alpha=0.004$. We have also found that the strains reaching 1% would result in the reduction of persistent currents by four orders of magnitude (not shown here). As long as the deformation occurs, no matter whether they are large or small, the abrupt jump structures of the persistent currents appearing at $\Phi_c=i\Phi_0$ for the undeformed torus would vanish, and the entire curve of the persistent current becomes a fully smooth analytic function of Φ. That is, they may be fitted well to $I=-A\sin(2\pi\Phi/\Phi_0)$, where $A=A(\varepsilon_L,\varepsilon_J,\tan\alpha,R,r,\theta)$, namely, the amplitude of the persistent current, is determined by the deformation and geometric parameters. The deformations induce the directional changing of the persistent currents and make paramagnetism of the undeformed torus at low magnetic flux Φ (in the range from 0 to $\Phi_0/2$) become diamagnetism, and the reverse change is also true for the flux between $\Phi_0/2$ and Φ_0. It is very important to note that if taking $\tan\alpha=0$ and $\varepsilon_L=\varepsilon_J$, the persistent current displays the same variation properties as that in the undeformed torus and its amplitude decreases very slightly as if there is no deformation occurring. This is the same reason as mentioned in Sec. II, i.e., such deformation would not change the geometrical symmetry of the graphite honeycomb structure. Therefore, it is confirmed again that the geometrical structure of carbon nanotorus is responsible for the electronic properties.

In order to further reveal the dependence of persistent current on the chirality and torus radius R in the existence of deformations, we define an increment of the persistent current as $\Delta I(\varepsilon_L,\Phi,T=0)=|I(\varepsilon_L,\Phi,T=0)|-|I(\varepsilon_L=0,\Phi,T=0)|$. The curves of $\Delta I(\varepsilon_L,\Phi,T=0)$ for various type I tori are shown in Fig. 5(c). The increment of persistent currents resulting from deformations is significantly affected by the chirality and dimension. The persistent current in an AZ

torus ($\theta=0$) drops less than that in other tori. We also find that the lesser the deviation of θ to $\pm 15°$, or the smaller the radius R of the deformed torus, the larger its persistent current dropping. These results can be understood in terms of the deformation-dependent energy gap for metallic nanotorus described in Sec. II and the persistent currents for the undeformed metallic nanotori shown in Sec. III A.

For the deformed type II torus, the dependence of the persistent currents on the deformed parameters $(\varepsilon_L, \varepsilon_J, \tan\alpha)$ at zero temperature is shown in Fig. 5(b). The similar results can be obtained as compared with the deformed type I torus. The very small deformation induces dramatic reduction of the persistent current, and the sawtooth shapes in the case of without deformation become smooth and can be fitted to $I=\pm A\sin(2\pi\Phi/\Phi_0)$, where the magnitude of amplitude A and sign $(+$ or $-)$ depend on the deformation parameters $(\varepsilon_L, \varepsilon_J, \tan\alpha)$ and geometric parameters (R, r, θ), that is, at low magnetic flux Φ (in the range from 0 to $\Phi_0/2$) the torus displaying paramagnetism or diamagnetism depends completely on the values of deformations. If taking $\tan\alpha=0$ and $\varepsilon_L=\varepsilon_J$, the persistent current remains almost the same value as that of the undeformed torus. Even if in the case of the smallest energy gap induced by deformations with some particular value (see Sec. II), the persistent currents are still weaker than that in the undeformed torus, suggesting that the persistent currents are determined not only by the electronic states nearest to Fermi level but also by the other electronic states far from Fermi level. In addition, in the deformed type II torus the increment of the persistent current is affected by chirality and radius, similar to the deformed type I torus.

IV. CONCLUSIONS

By using the unified expression of π-electron energy states as a function of chirality and deformations, the energy gaps and persistent currents for various carbon nanotori under the applied magnetic field are investigated. It has shown that the deformation-dependent energy gaps of various metallic tori display almost the same variation features for different deformation parameters $(\varepsilon_L, \varepsilon_J, \tan\alpha)$; whereas for various semiconducting tori the deformation-dependent energy gaps do not show the distinctive regularity associated with the deformation parameters and geometric parameters, but their energy gaps would be narrowed if the deformation parameters have some particular values.

For the undeformed metallic and semiconducting tori, the persistent currents versus the flux exhibit special jump structures. The current is strongly dependent on the chiral angle θ and becomes very strong as θ approaches $\pm 15°$. It is found that the persistent current is inversely proportional to the torus radius R but independent of torus width r and is very sensitive to deformation. When the strains reach 0.4%, the persistent current drops dramatically. No matter whether the deformations are large or not, the jump structures of the persistent currents become smooth and their curves may fit well to $I=\pm A\sin(2\pi\Phi/\Phi_0)$. When the strain reaches 1%, the persistent current almost vanishes. In the special case of $\tan\alpha=0$ and $\varepsilon_L=\varepsilon_J$, the persistent current remains almost the same value as that in the undeformed case.

Finally, we would like to point out if the circumference of carbon nanotorus is larger than the electron coherence length, especially the strong disorder is introduced into torus, even though it is undeformed, the persistent current also reduces to a very small magnitude[26] and is difficult to be observed.

ACKNOWLEDGMENTS

This work was supported by the National Natural Science Foundation of China (Grant Nos. 10304002 and 50372018), the Provincial Natural Science Foundation of Hunan (Grant No. 03JJY3013), the Doctoral Program Foundation of Ministry of Education of China (Grant No. 20030532008), and the Foundation of Excellent Ph.D thesis of Hunan Province (Grant No. 200526).

[1] S. J. Tans, M. H. Devoret, H. Dai, A. Thess, R. E. Smalley, L. J. Geerligs, and C. Dekker, Nature (London) **386**, 474 (1997).
[2] M. Bockrath, D. H. Cobden, P. L. McEuen, N. G. Chopra, A. Zettl, A. Thess, and R. E. Smalley, Science **275**, 1922 (1997).
[3] S. J. Tans, A. R. M. Verschueren, and C. Dekker, Nature (London) **393**, 49 (1998).
[4] K. Tsukagoshi, B. W. Alphenaar, and H. Ago, Nature (London) **401**, 572 (1999).
[5] P. G. Collins, A. Zettl, H. Bando, A. Thess, and R. E. Smalley, Science **278**, 100 (1997).
[6] M. S. Fuhrer *et al.*, Science **288**, 494 (2000).
[7] Z. Zhang, J. Peng, and H. Zhang, Appl. Phys. Lett. **79**, 3515 (2001).
[8] B. I. Dunlap, Phys. Rev. B **46**, 1933 (1992).
[9] S. Itoh, S. Ihara, and J. Kitakami, Phys. Rev. B **47**, 1703 (1993); **47**, 12908 (1993).
[10] B. M. Terrones, Philos. Trans. R. Soc. London, Ser. A **354**, 2025 (1992).
[11] J. Liu, H. Dai, J. H. Hafner, D. T. Colbert, R. E. Smalley, S. J. Tans, and C. Dekker, Nature (London) **385**, 780 (1997).
[12] R. Martel, H. R. Shea, and P. Avouris, Nature (London) **398**, 299 (1999); J. Phys. Chem. B **103**, 7551 (1999).
[13] M. Ahlskog, E. Seynaeve, R. J. M. Vullers, C. V. Haesendonck, A. Fonseca, K. Hernadi, and J. B. Nagy, Chem. Phys. Lett. **300**, 202 (1999).
[14] M. Sano, A. Kamino, J. Okamura, and S. Shinkai, Science **293**, 1299 (2001).
[15] H. R. Shea, R. Martel, and P. Avouris, Phys. Rev. Lett. **84**, 4441 (2000).
[16] H. Watanabe, C. Manabe, T. Shigematsu, and M. Shimizu, Appl. Phys. Lett. **78**, 2928 (2001).
[17] R. C. Haddon, Nature (London) **388**, 31 (1997).
[18] A. A. Kuzubov, Phys. Solid State **43**, 1982 (2001).
[19] V. Meunier, Ph. Lambin, and A. A. Lucas, Phys. Rev. B **57**, 14886 (1998).
[20] M. F. Lin and D. S. Chun, Phys. Rev. B **57**, 6731 (1998).
[21] M. F. Lin, J. Phys. Soc. Jpn. **67**, 1094 (1998).
[22] D.-H. Oh, J. M. Park, and K. S. Kim, Phys. Rev. B **62**, 1600 (2000).
[23] L. Liu, C. S. Jayanthi, and S. Y. Wu, Phys. Rev. B **64**, 033412 (2001).
[24] O. Hod, E. Rabani, and R. Baer, Phys. Rev. B **67**, 195408 (2003).
[25] A. Latge, C. G. Rocha, L. A. L. Wanderley, M. Pacheco, P. Orellana, and Z. Barticevic, Phys. Rev. B **67**, 155413 (2003).
[26] S. Latil, S. Roche, and A. Rubio, Phys. Rev. B **67**, 165420 (2000).
[27] P. R. Wallance, Phys. Rev. **71**, 622 (1947).
[28] R. Saito, G. Dresselhaus, and M. S. Dresselhaus, *Physical Properties of Carbon Nanotubes* (Imperial College Press, London, 1998).
[29] L. Chica, V. H. Crespi, L. X. Benedict, S. G. Louie, and M. L. Cohen, Phys. Rev. Lett. **76**, 971 (1996).
[30] Z. Z. Li, *Solid State Theory* (Higher Education Press, Beijing, China, 2002).
[31] S. Latil, S. Roche, and A. Rubio, Phys. Rev. B **67**, 165420 (2003).
[32] S. Roche and R. Saito, Phys. Rev. B **59**, 5242 (1999).
[33] J. M. Luttinger, Phys. Rev. **84**, 814 (1951).
[34] W. A. Harrison, *Electronic Structure and the Properties of Solids* (Dover, New York, 1989).
[35] Z. Zhang, J. Peng, X. Huang, and H. Zhang, Phys. Rev. B **66**, 085405 (2002).
[36] B. L. Altshuler, Y. Gefrn, and Y. Imry, Phys. Rev. Lett. **66**, 88 (1991).